Article

Not peer-reviewed version

Improved Electrochemical Performance of Li-Rich Cathode Materials via Spinel Li_2MoO_4 Coating

Shuhao Zhang , Yun Ye , Qinghao Lai , Tie Liu , Shuang Yuan *

Posted Date: 4 July 2023

doi: 10.20944/preprints202307.0029.v1

Keywords: LIBs; Li-rich manganese-based cathode material; Li2MoO4 coating; spinel phase; electrochemical performance

Article

Improved Electrochemical Performance of Li-Rich Cathode Materials via Spinel Li_2MoO_4 Coating

Shuhao Zhang [1], Yun Ye [1,2], Qinghao Lai [1], Tie Liu [3] and Shuang Yuan [1,*]

1 School of Metallurgy, Northeastern University, Shenyang 110819, China
2 Key Laboratory for Ecological Metallurgy of Multimetallic Mineral, Ministry of Education, Northeastern University, Shenyang 110819, China
3 Key Laboratory of Electromagnetic Processing of Materials (Ministry of Education), Northeastern University, Shenyang 110819, China
* Correspondence: yuans@smm.neu.edu.cn; Tel.: 86-024-83681171

Abstract: Li-rich manganese-based cathode materials (LRMs) are considered one of the most promising cathode materials for the next generation lithium-ion batteries (LIBs) because of their high energy density. However, there are problems such as capacity decay, poor rate performance, and continuous voltage drop, which seriously limit their large-scale commercial applications. In this work, $Li_{1.2}Mn_{0.54}Co_{0.13}Ni_{0.13}O_2$ coated with Li_2MoO_4 with unique spinel structure was prepared by wet chemistry method and the subsequent calcination process. The Li_2MoO_4 coating layer with spinel structure can provide a 3D Li^+ transport channel, which is beneficial for improving rate performance, while protecting LRMs from electrolyte corrosion, suppressing interface side reactions, and improving cycling stability. The capacity retention rate of LRMs coated with 3wt% Li_2MoO_4 increased from 69.25% to 81.85% after 100 cycles at 1C, and the voltage attenuation decreased from 7.06 to 4.98 mV per cycle. The lower R_{ct} also exhibits improved magnification performance. The results indicate that the Li_2MoO_4 coating effectively improves the cyclic stability and electrochemical performance of LRMs.

Keywords: LIBs; Li-rich manganese-based cathode material; Li_2MoO_4 coating; spinel phase; electrochemical performance

1. Introduction

LIBs as a kind of clean and renewable electrochemical energy storage equipment have been widely applied. However, the current energy density of commercial LIBs is insufficient to meet the growing demand, and the development of high-capacity electrode materials is urgent [1,2]. Li-rich manganese-based cathode materials (LRMs) are considered to be one of the most promising cathode materials for the next generation of LIBs due to their high specific capacity (>250 mAh/g), low cost, and excellent energy density (>1000 Wh/kg) [3,4]. The general formula of LRMs is $xLi_2MnO_3\cdot(1-x)$ $LiMO_2$ (M=Ni, Co, Mn). Based on the oxidation-reduction of transition metal ions (TM) and the additional oxygen redox, more Li can be removed to provide ultra-high capacity [5,6]. However, the practical application of LRMs is impeded by severe voltage and capacity decay, mainly due to continuous migration of transition metals (TM) and the resulting structural evolution from layered to spinel or rock salt phases [7,8].

TM migration or structural evolution begins on the surface of LRMs during the cycling process, so the surface protection of LRMs is crucial [9–11]. Surface coating is an effective surface protection method, which can protect electrode materials from electrolyte corrosion, inhibit oxygen release and stabilize crystal structure [12]. So far, many materials, such as oxides Al_2O_3 [13], ZrO_2 [14], fluoride AlF_3 [15], LiF [16], and metal phosphate $LiFePO_4$ [17], have been used as surface coatings to improve the cyclic stability of LRMs. However, although these efforts have made significant contributions to improving cycle life, most coatings have poor compatibility with LRMs, which is not conducive to uniform protection of LRMs and maintaining overall integrity with LRMs over long cycles [18].

 doi:10.20944/preprints202307.0029.v1

Therefore, it is highly desirable to introduce lithium-reactive coating materials to enhance the compatibility between the coating and the material body.

In this work, we coated a Li_2MoO_4 coating layer with a unique spinel structure on the surface of $Li_{1.2}Mn_{0.54}Co_{0.13}Ni_{0.13}O_2$. Through the wet chemistry method and the subsequent calcination process, Li_2MoO_4 can be evenly coated on the surface of LRMs. In addition, when molybdate reacts with the cathode material at high temperature, it can form spinel phase on the surface of the material by removing part of Li. The spinel structure has 3D Li^+ channels, which are conducive to Li^+ transport. At the same time, the Li_2MoO_4 coating as a good lithium ion conductor can provide better protection, preventing LRMs from electrolyte corrosion, thus improving structural stability and cycle life.

2. Materials and Methods

2.1. Materials Synthesis

The pristine $Li_{1.2}Mn_{0.54}Co_{0.13}Ni_{0.13}O_2$ were synthesized by a high temperature solid state method. In detail, the carbonate precursor ($Mn_{0.675}Co_{0.1625}Ni_{0.1625}CO_3$) from HaiAnZhiChuan Battery Materials Technology Co., LTD. was uniformly ground and mixed with Li_2CO_3 (an excess of 5% Li_2CO_3 was added to compensate for lithium loss during the elevated calcination step) in an agate mortar. Subsequently, the powder mixture was sintered at 500℃ for 6 h and then 850℃ for 12 h to produce the target $Li_{1.2}Mn_{0.54}Co_{0.13}Ni_{0.13}O_2$ (Pristine).

The prepared Li-rich cathode material was mixed with a certain amount of ammonium molybdate. To avoid agglomeration, the mixed materials were dissolved in absolute ethanol after grinding and stirred for 3 h. After evaporation in a water bath at 80℃, the desiccative powder was calcined at 720℃ for 4 h to obtain the Li_2MoO_4@$Li_{1.2}Mn_{0.54}Ni_{0.13}Co_{0.13}O_2$ sample. According to different contents of Li_2MoO_4, the prepared samples containing 1,3,5 wt% Li_2MoO_4 coating layer are termed 1wt%, 3wt% and 5wt%, respectively.

2.2. Material Characterization

X-ray diffraction patterns of samples for the crystal structure were obtained by X-ray powder diffractometer (XRD, D8 Advance, German Bruker AXS Co., LTD., Cu Kα radiation), and XRD data were obtained in an angular range of 10-80° with a scanning speed of 1°/min. The test results were refined using GSAS [19]. Scanning electron microscopy (SEM, Thermo Scientific Apreo 2c) was applied to observe the morphology of the material. Transmission electron microscopy (TEM, JEM2200FS) was used to detect the structure and microstructure of the samples. The inductively coupled plasma emission spectrometer (ICP-OES, Agilent 5110) was used to determine the composition of the elements. X-ray photoelectron spectroscopy analyzer (XPS, Thermo ESCALAB 250XI) was used to measure element species and valence state information on the sample surface.

2.3. Electrochemical Characterization

The active cathode material, acetylene black, and PVDF binder (mass ratio of 8:1:1) were mixed and dispersed in N-methyl-2-pyrrolidone (NMP) solvent to prepare the cathode slurry, which was then coated on Al foil and dried at 60℃ for 12 h in a oven. The dried electrode was cut into a round film with a diameter of 12 mm and the weight loading of the active materials was about 1.5 mg/cm. The test cells were assembled as CR2025-type coin cells in an Ar glove box (H_2O and O_2 content below 0.1 ppm), and a high voltage electrolyte (LB-111, Duoduo Company) was used as the electrolyte. Electrochemical measurements of the assembled cells were carried out on a LAND at a temperature of 30 °C. The batteries were tested in the voltage range of 2.0-4.8 V. For 1 C (1 C=250 mA/g) cycling tests, the batteries were first cycled at 0.1 C three times and then cycled to 100 cycles at 1 C. The rate performance of the batteries was tested at 0.1, 0.2, 0.5, 1, 2, and 5 C, and then returned to 0.1 C. CV was conducted on a VSP electrochemical workstation at a voltage between 2.0 and 4.8 V at a scan rate of 0.1 mV/s. Electrochemical impedance spectroscopy (EIS) was performed on a VSP electrochemical workstation at a frequency range of 0.01 Hz-100 Hz and an AC amplitude of 5 mV.

Preprints (www.preprints.org) | NOT PEER-REVIEWED | Posted: 4 July 2023 doi:10.20944/preprints202307.0029.v1

3. Results and Discussion

3.1. Material Characterizations

The inductively coupled plasma optical emission spectrometer (ICP-OES) analysis was used to investigate the cation ratio of as-obtained cathode materials, and the results are listed in Table S1. The results indicate that the experimental results are in good agreement with the design values.

Figure 1 shows the X-ray powder diffraction (XRD) patterns of the samples and their Rietveld refinement results. Figure 1 indicates the presence of a lamellar α-$NaFeO_2$ structure with the R-3m space group in the four samples, and the characteristic peak in the range of 20-25° also demonstrates the presence of the Li_2MnO_3 phase with the C2/m space group in the samples. The clear split of the (006)/(102) and (108)/(110) peaks implies a highly ordered layered structure of the samples [20]. In addition, other peaks can be clearly observed near 18, 30, and 35°, and the peak intensity increases with the increase of Li_2MoO_4 coating amount. After analysis and comparison, it can be determined that the weak peak is the spinel structure of Li_2MoO_4 (Figure S1 [21]).

we performed a Rietveld refinement on the XRD curves of four samples using a two-phase structure model consisting of rhomboidal R-3m and monoclinic C2/m phases, and the results are shown in Figure 1b-e. According to reports, the diffraction peak intensity ratio between the planes (003) and (104) can be used to estimate the degree of Li/Ni mixing. The smaller the ratio, the greater the degree of Li/Ni mixing [22]. As shown in Table 1, the ratios I(003)/I(104) of all samples are greater than 1.2, indicating a lower Li/Ni miscibility [23]. Compared to the original sample, the ratio I(003)/I(104) of the sample coated with Li_2MoO_4 decreased slightly, possibly due to the intensification of Li/Ni mixing during high-temperature calcination during the preparation process. Among them, the ratio I(003)/I(104) of the 3wt% sample is closest to the original sample, and the content of Ni^{2+}in the Li layer in the refined results of Table 1 also corresponds to the ratio I(003)/I(104). Additionally, the spacing between layers of the sample coated with Li_2MoO_4 increased slightly, possibly due to partial doping of Mo in the TM layer on the surface. The subsequent X-ray photoelectron spectroscopy (XPS) results provide evidence for this result. However, the ratio between the lattice parameters c and a of the four samples is greater than 4.99, indicating that the samples have a fine-layered structure [24]. At the same time, the content of Li_2MoO_4 in the coated samples was refined and the results are shown in Table 1. Except for the low peak intensity of Li_2MoO_4 in the 1wt% sample, which cannot obtain the content of Li_2MoO_4, the content of Li_2MoO_4 in the 3wt% and 5wt% samples is in good agreement with the design values and ICP results.

The morphological characteristics of the prepared samples were investigated by scanning electron microscope (SEM), and the obtained images are shown in Figure S2. The morphology of all the sample particles is spherical and the diameter of the secondary particles ranges from 10 to 15 μm. Primary particles can be clearly seen on the surface of the original sample particles, but the surface of the coated Li-rich material becomes smooth.

Preprints (www.preprints.org) | NOT PEER-REVIEWED | Posted: 4 July 2023 doi:10.20944/preprints202307.0029.v1

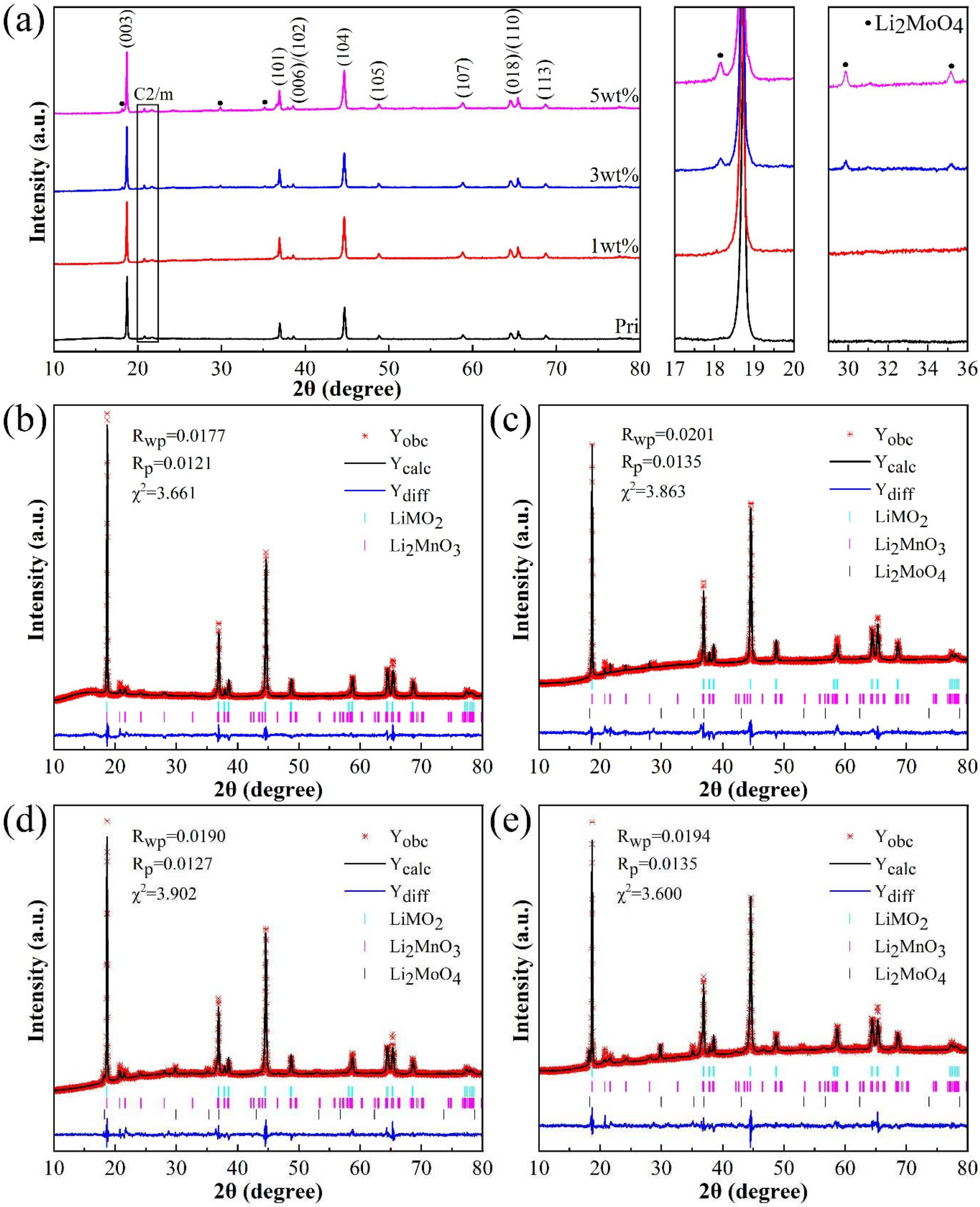

Figure 1. (a) XRD patterns and enlarged XRD patterns in selected 2θ range of four samples. (b-e) Rietveld refinement of XRD patterns.

Table 1. Lattice parameters of samples from Rietveld refinement.

Samples	$I_{(003)}I_{(104)}$	c	a	c/a	Ni^{2+}in Li layer (%)	Li_2MoO_4 content (wt%)
Pristine	1.692	14.245782	2.854563	4.990529899	3.83	0
1wt%	1.258	14.257465	2.855348	4.993249509	5.36	-
3wt%	1.526	14.248178	2.854860	4.990849989	3.88	3.0158
5wt%	1.332	14.262967	2.856606	4.992976630	4.30	4.7180

 doi:10.20944/preprints202307.0029.v1

Transmission electron microscope (TEM) and fast Fourier transform (FFT) were performed to display the crystal structure near the surface areas of the 3wt% sample. The Li_2MoO_4 coating layers on the surface of the material can be clearly observed in Figure 2a. Figure 2b shows clear lattice stripes of the layered structure. Combining with the FFT image (Figure 2e) of the corresponding position in Figure 2d, it can be determined that the spacing of lattice stripes is 0.474 nm, which is very consistent with the plane (003) of the R-3m space group of the li-rich layered structure. Through the analysis of the FFT image of the blue region in Figure 2c, it can be found that a spinel structure coating is formed on the surface of the material coated with Li_2MoO_4. The thickness of the coating can reach over 20 nm due to not only the unique spinel structure of Li_2MoO_4 formed by coating, but also the spinel phase formed by the detachment of some Li from the material surface during the formation of Li_2MoO_4 coating [21]. To further investigate the existence of the Li_2MoO_4 coating layer on the surface of 3wt% sample, EDS was carried out and the corresponding elemental mapping is shown in Figure 2f-k. The elements of Mn, Co, Ni, O, and Mo are evenly distributed on the particle, illustrating that the Li_2MoO_4 layer was successfully coated on the bulk material.

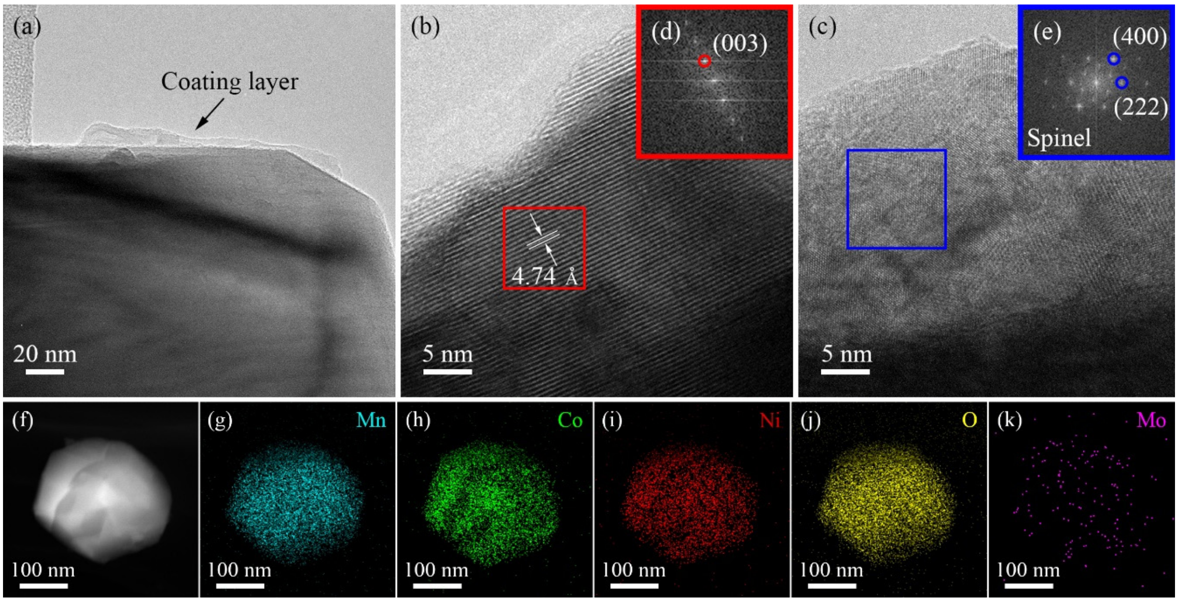

Figure 2. (a) TEM image of 3wt% sample, (b, c) TEM images of the internal layered structure and the surface spinel structure coating layer of the 3wt% sample, respectively, and (d, e) FFT images of the red area in (b) and the blue area in (c), respectively. (f) TEM image of 3wt% sample, and (g-k) EDS mapping of Mn, Co, Ni, O, and Mo.

X-ray photoelectron spectroscopy (XPS) measurements were performed to confirm the composition of the surface elements and the chemical state of the Pristine and 3wt% samples (Figure 3 and Figure S2). Figure 3a and b present the XPS full spectra of the Pristine and 3wt% sample, respectively. Figure 3c shows that the 3wt% sample had a Mo 3d photoelectron emission intensity peak near 232 eV and235 eV, which corresponded to Mo $3d_{5/2}$ and Mo $3d_{3/2}$, respectively, indicating that Mo^{6+} on the surface of 3wt% sample may be in the form of Li_2MoO_4, and the presence of Mo^{4+} indicates that some Mo^{6+} is doped in the lattice interior to convert to Mo^{4+} to maintain electroneutrality [25]. Figure S2 presents the XPS spectra of Mn, Co, and Ni elements for Pristine and 3wt% sample, respectively. The valence states of Mn, Co, and Ni do not change greatly, which indicates that the coating maintains the original system status of the Li-rich materials.

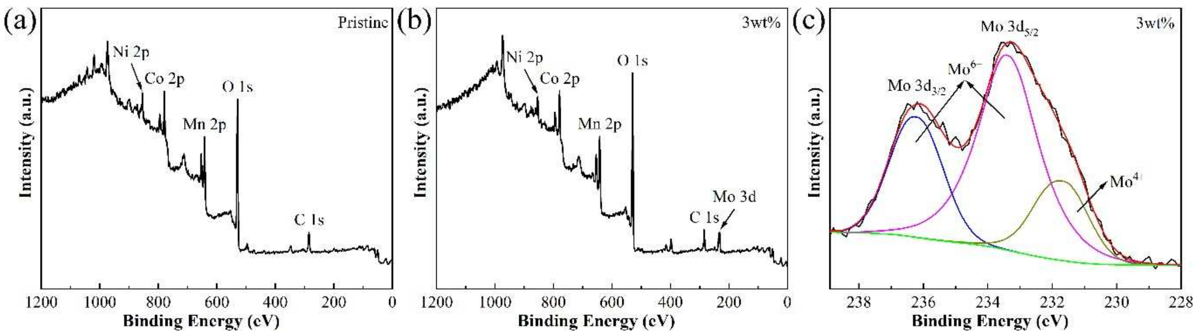

Figure 3. (a-b) XPS full spectrum for Pristine and 3wt% samples, and (c) XPS spectra of Mo 3d for 3wt% sample.

3.2. Electrochemical Performances

Figure 4a shows the initial charge-discharge curves of the four samples (2.0-4.8 V, 0.1 C). During the first discharge, the Pristine, 1wt%, 3wt%, and 5wt% sample release 259.65, 250.29, 257.31 and 248.74 mAh/g, respectively, corresponds to Coulombic efficiencies of 56.66, 76.92, 77.79 and 75.16%. All samples show the typical initial charge process of Mn-based lithium-rich cathode materials. In detail, the charge curve can be divided into two parts, a sloping part below 4.5 V and a long plane part at 4.5 V. The sloping region belongs to the oxidation reaction of Ni^{2+}/Ni^{4+} and Co^{3+}/Co^{4+}, while the long plateau is related to the oxygen activation of Li_2MnO_3 [26]. Compared to the original sample, the platform of the sample coated with Li_2MoO_4 becomes shorter near 4.5 V. This is because the formation of the Li_2MoO_4 coating layer removes some Li from the material and pre-activates the Li_2MnO_3 component [27,28]. Therefore, the sample coated with Li2MoO4 has a higher initial Coulombic efficiency. The cyclic performance of four samples at 1 C is shown in Figure S4b. For comparison purposes, only the cyclic performance of the Pristine and 3wt% samples is shown in Figure 4b. The results showed that the Li_2MoO_4 coating improved the cycling performance of the material, with only 69.25% capacity retention rate of the original sample after 100 cycles, while the 3wt% sample still had 81.85% capacity retention rate after 100 cycles.

Figure 4c shows the rate performance of the samples. The discharge capacity of all four samples decreases with the increase of current density, with a 3wt% sample exhibiting the best rate performance. The spinel has a 3D Li^+ channel compared to the 2D Li^+ channel of the LRMs, which favors an improvement in the rate capability [29]. Meanwhile, Li_2MoO_4 belongs to the fast-ion conductor, which is conducive to Li^+ transport. Therefore, the material coated with Li_2MoO_4 has higher rate performance [30].

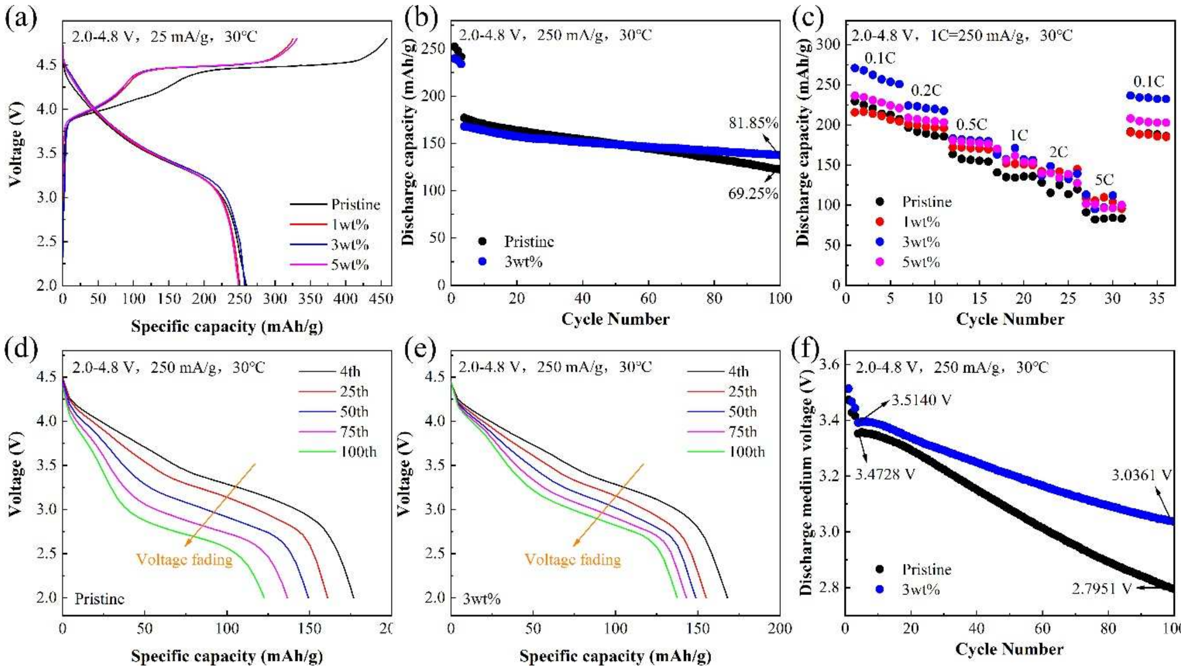

Figure 4. (a) Initial charge-discharge curves of four samples at 0.1 C, (b) Cycle performance for Pristine and 3wt% sample. (c) Rate capacity of four samples. (d, e) Attenuation of discharge voltage for Pristine and 3wt% sample, and (f) discharge medium voltage attenuation curves for Pristine and 3wt% sample.

In addition, according to Figure 4d and e, the Pristine sample exhibits faster voltage and capacity decay, which is also one of the main problems of Li-rich materials. Figure 4f shows that the average voltage decay of the 3wt% sample (voltage drop of 4.98 mV per cycle, 100 cycles) is less than that of the Pristine sample (voltage drop of 7.06 mV per cycle, 100 cycles) at high cutoff voltage (4.8 V). The increase in capacity and discharge voltage retention of the 3wt% sample is due to the effective reduction of direct contact between the electrode and the electrolyte by the Li_2MoO_4 coating, which inhibits the erosion of Li-rich materials during discharge, prevents the oxidation of the electrolyte on the surface of the cathode material during charging, and improves its structural stability.

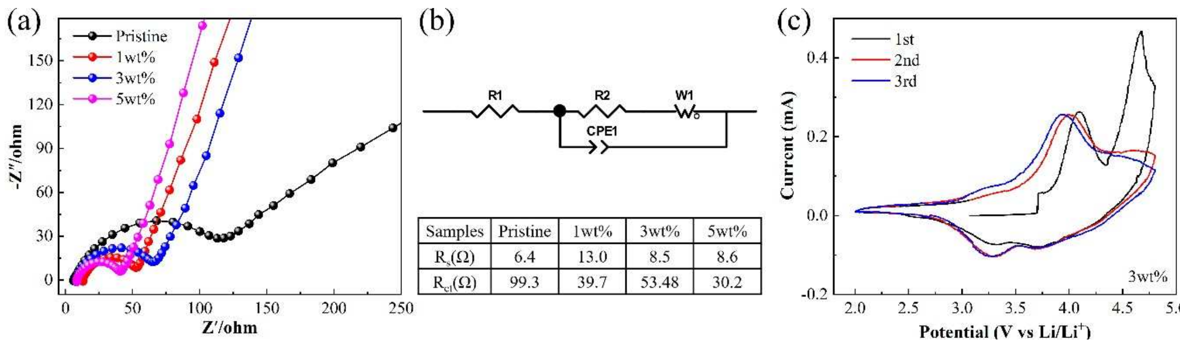

Figure 4. (a) AC impedance spectra of four samples, and (b) equivalent circuit diagram and impedance parameters of the samples. (c) CV curves of 3wt% sample.

In order to investigate the kinetic properties of the prepared samples, the electrochemical impedance spectroscopy (EIS) measurement was conducted. As shown in Figure 5a, the impedance curve consists of a semicircle whose diameter represents the charge transfer resistance (R_{ct}) and the oblique line represents the Warburg impedance. The equivalent circuit and the impedance parameters fitted to four samples are shown in Figure 5b. As expected, R_{ct} decreased after coating

Preprints (www.preprints.org) | NOT PEER-REVIEWED | Posted: 4 July 2023 doi:10.20944/preprints202307.0029.v1

with Li_2MoO_4, which was attributed to the spinel structure of the Li_2MoO_4 coating that is capable of providing 3D channels for Li^+ diffusion, which is favorable for Li^+ diffusion.

Figure 5c shows the CV curve of the 3wt% sample between 2.0-4.8 V. During the initial charge and discharge cycle, the CV curve exhibits two different oxidation processes, corresponding to the oxidation reaction of Ni^{2+}/Ni^{4+} and Co^{3+}/Co^{4+}, and the activation of the Li_2MnO_3 phase, respectively. When the voltage is higher than 4.5 V, the deintercalation of Li would be accompanied by the release of oxygen, but there is no oxidation peak at 4.68 V in the subsequent cycles [31]. The activation of the Li_2MnO_3 phase occurs only during the first charge discharge cycle, which is also the reason for the low initial Coulombic efficiency of Li-rich materials.

4. Conclusions

In summary, $Li_{1.2}Mn_{0.54}Co_{0.13}Ni_{0.13}O_2$ coated with Li_2MoO_4 was successfully prepared. XRD results indicate that the samples coated with Li_2MoO_4 exhibit a good layered structure, while the Li_2MoO_4 coating exhibits a unique spinel structure. The SEM and TEM results indicate that Li_2MoO_4 is perfectly coated on the surface of the material. To determine the optimal amount of coating, a series of Li-rich materials coated with Li_2MoO_4 were prepared, among which the 3wt% Li_2MoO_4 sample exhibited the best electrochemical performance. Compared to the Pristine sample, the initial Coulomb efficiency of the sample coated with Li_2MoO_4 has greatly improved, from 56.66% to over 75%, effectively alleviating the problem of low initial Coulomb efficiency in Li-rich materials. After 100 cycles at 1 C, the original sample only had a capacity retention rate of 69.25%, while the sample coated with 3wt% Li_2MoO_4 had a capacity retention rate of 81.85%, greatly improving cycling performance. Meanwhile, the magnification performance curve also indicates that the sample coated with 3wt% Li_2MoO_4 has higher capacity at high magnification. Furthermore, the voltage attenuation of Li-rich materials coated with Li_2MoO_4 was also suppressed. Compared to the original sample, the voltage attenuation of the sample coated with 3wt% Li_2MoO_4 slowed by an average of 2.08 mV per 100 cycles. The EIS results showed that the R_{ct} of the sample coated with Li_2MoO_4 decreased significantly and the diffusion of Li^+ was enhanced. This work indicates that the Li_2MoO_4 coating can enhance the cyclic stability of Li-rich materials and improve their electrochemical performance.

Supplementary Materials: The following supporting information can be downloaded at: www.mdpi.com/xxx/s1, Table S1: Composition of cational elements in sample Pristine, 1wt%, 3wt% and 5wt% as measured by ICP-OES; Table S2: ICP-OES results of the obtained samples. Figure S1: XRD spectrum analysis of spinel Li_2MoO_4 phase; Figure S2: SEM images for (a) Pristine, (b) 1wt%, (c) 3wt%, (d) 5wt%; XPS spectra of (a) Mn 2p, (b) Co 2p, and (c) Ni 2p for Pristine and 3wt% sample; Figure S3: XPS spectra of (a) Mn 2p, (b) Co 2p, and (c) Ni 2p for Pristine and 3wt% sample; Figure S4: The cyclic performance (a) and capacity retention rate (b) of four samples at 1C.

Author Contributions: Conceptualization, S.Z. and S.Y.; methodology, S.Z. and Y.Y.; formal analysis, Q.L.; investigation, S.Z.; data curation, Y.Y.; writing—original draft preparation, S.Z.; writing—review and editing, Q. L and T.L.; supervision, S.Y.; project administration, S.Y.; funding acquisition, S.Y. All authors have read and agreed to the published version of the manuscript.

Funding: This work is supported by the National Natural Science Foundation of China (Grant No. 52274294), the Fundamental Research Funds for the Central Universities (Grant No. N2124007-1).

Institutional Review Board Statement: Not applicable.

Informed Consent Statement: Not applicable.

Data Availability Statement: Not applicable.

Conflicts of Interest: The authors declare no conflict of interest.

References

1. Liu J, Wang J, Ni Y, Zhang K, Cheng F, Chen J. Recent breakthroughs and perspectives of high-energy layered oxide cathode materials for lithium ion batteries. Materials Today, 2021, 43: 132-165.
2. Wang M J, Yu F D, Sun G, Wang J, Zhou J G, Gu D M, Wang Z B. Co-regulating the surface and bulk structure of Li-rich layered oxides by a phosphor doping strategy for high-energy Li-ion batteries. Journal of Materials Chemistry A, 2019, 7(14): 8302-8314.

3. Lin T G, Seaby T, Hu Y X, Ding S S, Liu Y, Luo B, Wang L Z. Understanding and Control of Activation Process of Lithium-Rich Cathode Materials. Electrochemical Energy Reviews, 2022, 5(SUPPL 2).
4. Mei J, Chen Y Z, Xu W J, He W, Wang L, Xie Q S, Peng D L. Multi-strategy synergistic Li-rich layered oxides with fluorine-doping and surface coating of oxygen vacancy bearing CeO2 to achieve excellent cycling stability. Chemical Engineering Journal, 2022, 431.
5. Zheng H F, Hu Z Y, Liu P F, Xu W J, Xie Q S, He W, Luo Q, Wang L S, Gu D D, Qu B H, Zhu Z Z, Peng D L. Surface Ni-rich engineering towards highly stable $Li_{1.2}Mn_{0.54}Ni_{0.13}Co_{0.13}O_2$ cathode materials. Energy Storage Materials, 2020, 25: 76-85.
6. Huang Z, Xiong T F, Lin X, Tian M Y, Zeng W H, He J W, Shi M Y, Li J N, Zhang G B, Mai L Q, Mu S C. Carbon dioxide directly induced oxygen vacancy in the surface of lithium-rich layered oxides for high-energy lithium storage. Journal of Power Sources, 2019, 432: 8-15.
7. Liu S, Liu Z P, Shen X, Li W H, Gao Y R, Banis M N, Li M S, Chen K, Zhu L, Yu R C, Wang Z X, Sun X L, Lu G, Kong Q Y, Bai X D, Chen L Q. Surface Doping to Enhance Structural Integrity and Performance of Li-Rich Layered Oxide. Advanced Energy Materials, 2018, 8(31).
8. Ji X Q, Xia Q, Xu Y X, Feng H L, Wang P F, Tan Q Q. A review on progress of lithium-rich manganese-based cathodes for lithium ion batteries. Journal of Power Sources, 2021, 487.
9. Luo D, Cui J X, Zhang B K, Fan J M, Liu P Z, Ding X K, Xie H X, Zhang Z H, Guo J J, Pan F, Lin Z. Ti-Based Surface Integrated Layer and Bulk Doping for Stable Voltage and Long Life of Li-Rich Layered Cathodes. Advanced Functional Materials, 2021, 31(14).
10. He W, Guo W, Wu H, Lin L, Liu Q, Han X, Xie Q, Liu P, Zheng H, Wang L, Yu X, Peng D-L. Challenges and Recent Advances in High Capacity Li-Rich Cathode Materials for High Energy Density Lithium-Ion Batteries. Advanced Materials, 2021, 33(50).
11. Peng J M, Li Y, Chen Z Q, Liang G M, Hu S J, Zhou T F, Zheng F H, Pan Q C, Wang H Q, Li Q Y, Liu J W, Guo Z P. Phase Compatible $NiFe_2O_4$ Coating Tunes Oxygen Redox in Li-Rich Layered Oxide. Acs Nano, 2021, 15(7): 11607-11618.
12. Kim J M, Zhang X H, Zhang J G, Manthiram A, Meng Y S, Xu W. A review on the stability and surface modification of layered transition-metal oxide cathodes. Materials Today, 2021, 46: 155-182.
13. Hall D S, Gauthier R, Eldesoky A, Murray V S, Dahn J R. New Chemical Insights into the Beneficial Role of Al_2O_3 Cathode Coatings in Lithium-ion Cells. Acs Applied Materials & Interfaces, 2019, 11(15): 14095-14100.
14. Zhou Z W, Luo Z Y, He Z J, Zheng J C, Li Y J, Yan C, Mao J. Suppress voltage decay of lithium-rich materials by coating layers with different crystalline states. Journal of Energy Chemistry, 2021, 60: 591-598.
15. Zheng J M, Gu M, Xiao J, Polzin B J, Yan P, Chen X L, Wang C M, Zhang J G. Functioning Mechanism of AlF_3 Coating on the Li- and Mn-Rich Cathode Materials. Chemistry of Materials, 2014, 26(22): 6320-6327.
16. Ding X, Li Y X, Chen F, He X D, Yasmin A, Hu Q, Wen Z Y, Chen C H. In situ formation of LiF decoration on a Li-rich material for long-cycle life and superb low-temperature performance. Journal of Materials Chemistry A, 2019, 7(18): 11513-11519.
17. Zheng F H, Yang C H, Xiong X H, Xiong J W, Hu R Z, Chen Y, Liu M L. Nanoscale Surface Modification of Lithium-Rich Layered-Oxide Composite Cathodes for Suppressing Voltage Fade. Angewandte Chemie-International Edition, 2015, 54(44): 13058-13062.
18. Zhang X D, Shi J L, Liang J Y, Yin Y X, Zhang J N, Yu X Q, Guo Y G. Suppressing Surface Lattice Oxygen Release of Li-Rich Cathode Materials via Heterostructured Spinel $Li_4Mn_5O_{12}$ Coating. Advanced Materials, 2018, 30(29).
19. Toby B H. EXPGUI, a graphical user interface for GSAS. Journal of Applied Crystallography, 2001, 34: 210-213.
20. Pang W K, Lin H F, Peterson V K, Lu C Z, Liu C E, Liao S C, Chen J M. Effects of Fluorine and Chromium Doping on the Performance of Lithium-Rich $Li_{1+x}MO_2$ (M=Ni, Mn, Co) Positive Electrodes. Chemistry of Materials, 2017, 29(24): 10299-10311.
21. Zhu Z, Gao R, Waluyo I, Dong Y H, Hunt A, Lee J, Li J. Stabilized Co-Free Li-Rich Oxide Cathode Particles with An Artificial Surface Prereconstruction. Advanced Energy Materials, 2020, 10(35).
22. Yi L H, Liu Z S, Yu R Z, Zhao C X, Peng H F, Liu M H, Wu B, Chen M F, Wang X Y. Li-Rich Layered/Spinel Heterostructured Special Morphology Cathode Material with High Rate Capability for Li-Ion Batteries. Acs Sustainable Chemistry & Engineering, 2017, 5(11): 11005-11015.
23. Lou M, Zhong H, Yu H T, Fan S S, Xie Y, Yi T F. $Li_{1.2}Mn_{0.54}Ni_{0.13}Co_{0.13}O_2$ hollow hierarchical microspheres with enhanced electrochemical performances as cathode material for lithium-ion battery application. Electrochimica Acta, 2017, 237: 217-226.
24. Zheng H F, Zhang C Y, Zhang Y G, Lin L, Liu P F, Wang L S, Wei Q L, Lin J, Sa B S, Xie Q S, Peng D L. Manipulating the Local Electronic Structure in Li-Rich Layered Cathode Towards Superior Electrochemical Performance. Advanced Functional Materials, 2021, 31(30).
25. Teng T, Xiao L, Shen L, Ran J J, Xiang G, Zhu Y R, Chen H. Simultaneous Li_2MoO_4 coating and Mo^{6+} doping improves the structural stability and electrochemical properties of nickel-rich $LiNi_{0.83}Co_{0.11}Mn_{0.06}O_2$. Applied Surface Science, 2022, 601.

26. Yang P H, Zhang S C, Wei Z W, Guan X G, Xia J, Huang D Y, Xing Y L, He J, Wen B H, Liu B, Xu H Z. A Gradient Doping Strategy toward Superior Electrochemical Performance for Li-Rich Mn-Based Cathode Materials. Small, 2023.
27. Zheng J, Deng S N, Shi Z C, Xu H J, Xu H, Deng Y F, Zhang Z, Chen G H. The effects of persulfate treatment on the electrochemical properties of $Li[Li_{0.2}Mn_{0.54}Ni_{0.13}Co_{0.13}]O_2$ cathode material. Journal of Power Sources, 2013, 221: 108-113.
28. Guo W B, Zhang C Y, Zhang Y G, Lin L, He W, Xie Q S, Sa B S, Wang L S, Peng D L. A Universal Strategy toward the Precise Regulation of Initial Coulombic Efficiency of Li-Rich Mn-Based Cathode Materials. Advanced Materials, 2021, 33(38).
29. Zhu W, Tai Z G, Shu C Y, Chong S K, Guo S W, Ji L J, Chen Y Z, Liu Y N. The superior electrochemical performance of a Li-rich layered cathode material with Li-rich spinel $Li_4Mn_5O_{12}$ and MgF_2 double surface modifications. Journal of Materials Chemistry A, 2020, 8(16): 7991-8001.
30. Ren X Y, Du J L, Pu Z H, Wang R B, Gan L, Wu Z. Facile synthesis of Li_2MoO_4 coated $LiNi_{1/3}Co_{1/3}Mn_{1/3}O_2$ composite as a novel cathode for high-temperature lithium batteries. Ionics, 2020, 26(4): 1617-1627.
31. Chen J X, Huang Z, Zeng W H, Ma J J, Cao F, Wang T T, Tian W X, Mu S C. Surface Engineering and Trace Cobalt Doping Suppress Overall Li/Ni Mixing of Li-rich Mn-based Cathode Materials. Acs Applied Materials & Interfaces, 2022, 14(5): 6649-6657.